Received September 29, 2018, accepted October 16, 2018, date of publication October 22, 2018,
date of current version November 30, 2018.

Digital Object Identifier 10.1109/ACCESS.2018.2877364

Probability of Detection of the Angle of Arrival for Massive MIMO Arrays

CLAUDIO ALFONSO BOHÓRQUEZ CAMARGO[1], GUSTAVO FRAIDENRAICH[1], AND LUCIANO LEONEL MENDES[2]

[1]Faculdade de Engenharia Elétrica e de Computação, Universidade Estadual de Campinas, UNICAMP, Campinas 13083-852, Brazil
[2]Centro de Referência em Radiocomunicações, Instituto Nacional de Telecomunicações, INATEL, Santa Rita do Sapucaí 37540-0000, Brazil

Corresponding author: Gustavo Fraidenraich (gf@decom.fee.unicamp.br)

The work of C. A. Bohórquez Camargo was supported by CAPES. The work of G. Fraidenraich was supported by CNPq under Grant 304946/2016-8.

ABSTRACT In massive multiple input multiple output systems, where a large number of antennas are used, the dependency of the power spectrum on the signal direction allows angle-of-arrival (AoA) estimation with a very high precision. In this paper, we derive the probability to correctly detect the AoA using the conventional beamformer. The derivation is presented in an exact manner for uniform linear arrays and uniform rectangular array geometries. The resulting expressions depend on the noise power, fading variance, the number of signal snapshots, and the number of antennas. We have numerically evaluated the simulated and analytical probability of detection and they have shown a perfect agreement for distinct scenarios.

INDEX TERMS Angle of arrival, beamforming, probability of detection, ULA, URA, massive MIMO.

I. INTRODUCTION

The upcoming fifth generation (5G) of mobile network communication technology is considering the use of Massive MIMO (large number of antennas) at the base station. Research in the Massive MIMO subject has investigated many different areas such as architecture, channel modeling, power allocation, parallel models (D2D Device to Device communications), performance analysis, fading behavior, and channel state information (CSI) [1]–[4]. However, there are few works [5] where Massive MIMO system is used for localization of terminals.

There are several techniques for device localization. Among the most important, we can enumerate the following:

- **Time of Arrival (ToA)**, which uses the delay principle in signal transmission and matched filter for time/distance estimation [6].
- **Angle of Arrival (AoA)**, which uses the signal delay between elements of an antenna array and/or the correlation of power and direction of arrival of a group of signals [7]–[10].
- **Received Signal Strength (RSS)**, which uses the relationship between distance and power of a signal transmitted in a physical medium [11], [12].
- **Hybrid approaches**, which employ simultaneous available data from previously mentioned methods [5], [13].

Usually, all the described approaches, work as inputs for localization applications where the final output is a position or a distance. Typical works in these applications investigate the development of new algorithms using procedures like Least Squares [14], Kalman filters [15] or fingerprint methods [16]. In the mentioned cases, the performance is assessed using metrics like position/angle RMSE (Root Mean Square Error) versus signal to noise ratio (SNR), number of antennas, or bandwidth [6].

Massive MIMO takes advantage of a large number of antennas to decrease the effect of noise and fading [1]. In the Marzetta's [4] pioneer paper, it has been shown that the use of the conventional beamforming technique is optimal as the number of antennas increases. It turns out that this basic technique for AoA estimation is the same used for combining the signals in the Massive MIMO system.

Several works have proposed algorithms and assessment methods for AoA estimation [7]–[10], [14], [15], however, to the best of our knowledge, the probability of detection for AoA using the conventional beamformer is unavailable in the literature.

There are other AoA estimation techniques such as Capon [17], MUSIC (Multiple Signal Classification) [18], ESPRIT (Estimation of Signal Parameters via Rotational Invariance Technique) [19], and RiMAX [20], that present better performance than the basic method investigated here.

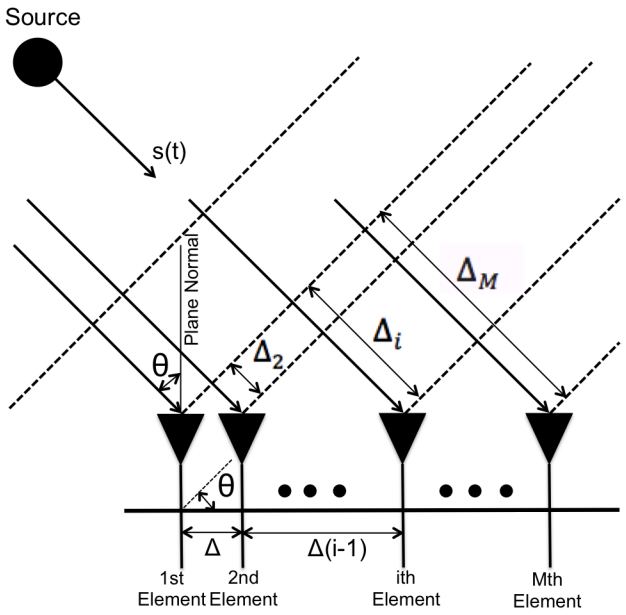

FIGURE 1. Physical model of an ULA system with *M* antennas.

However, the connection to Massive MIMO technique plays a key role that has motivated the derivation of the proposed metric. In fact, we have also tried to derive the same metric for MUSIC and Capon techniques, however, these calculations are quite involved and would require new developments in invertible non-central complex Wishart matrices, supersymmetry (use of anticommuting variables) and complex eigenvectors PDF (Probability Density Function) [7], [21]. In this way, we can say that our derived expressions can be used as a lower bound or an approximation to estimate the probability of detection for other techniques.

In this work, we derive the probability of detection for AoA using conventional beamforming in fading and noise scenarios for ULA and URA geometries. Our derived expressions are presented as a function of the number of signal snapshots, the magnitude of fading variance, the magnitude of noise variance, and the number of antennas.

The paper is organized as follows: Section II presents the system model. Section III formulates the problem for probability of detection. Section IV illustrates the derivation of the probability of detection for ULA and URA cases. Section V exhibits numerical results (analytical and simulated) for the probability of detection. Finally, some conclusions are drawn in the Conclusions section.

II. SYSTEM MODEL

Fig. 1 shows a typical ULA system where the signal received by the i-th antenna element is given as

$$r_i(t) = s(t)h_i(t)e^{j(i-1)\mu(\theta)} + n_i(t), \tag{1}$$

where $s(t)$ is the transmitted signal, $\mu(\theta) = \frac{2\pi}{\lambda}\Delta\sin(\theta)$ is the spatial frequency, $h_i(t)$ models the fading, λ is the wavelength, Δ is the distance between elements, $n_i(t)$ is the additive Gaussian noise, and θ is the AoA of the direct line of sight component. The signal received by all the elements of the array can be written in a $1 \times M$ vector form as

$$\mathbf{r}(t) = \widetilde{\mathbf{a}}(\theta) \circ \mathbf{h}(t)s(t) + \mathbf{n}(t), \tag{2}$$

where the symbol $\circ$ stands for the Hadamard product, and the steering vector $\widetilde{\mathbf{a}}$ is given as

$$\widetilde{\mathbf{a}}(\theta) = \frac{\mathbf{a}(\theta)}{\sqrt{M}} = \frac{1}{\sqrt{M}}\left[1 e^{j\mu(\theta)} \dots e^{j(M-1)\mu(\theta))}\right], \tag{3}$$

the fading vector $\mathbf{h}(t)$ is a complex Gaussian random process with unitary mean ($\mu_f = 1$) for the real and imaginary part, and covariance matrix $\sigma_f^2\mathbf{I}_M$, where $\mathbf{I}_M$ stands for a $M \times M$ identity matrix. Namely, the channel for signal $s(t)$ is set as Rician fading with a dominant LoS component, i.e. μ_f. The noise $\mathbf{n}(t)$ is a complex noise random process with zero mean and covariance matrix $\sigma_n^2\mathbf{I}$.

The sample covariance matrix can be used to calculate the degree of correlation between a group of signals. The higher the value of the matrix elements, the higher the degree of correlation between the signals. Signals arising from the same origin are highly correlated and therefore the sample covariance matrix $\mathbf{R}$ can be used to estimate the angle of arrival, as vastly reported in many references [7], [22]–[24].

Assuming a specific time t_k, we define $\mathbf{r}_k = \mathbf{r}(t = t_k)$, and therefore the covariance matrix can be written as

$$\mathbf{R} = \frac{1}{K}\sum_{k=0}^{K-1}\mathbf{r}_k^H\mathbf{r}_k, \tag{4}$$

where $(\cdot)^H$ stands for the conjugate transpose or Hermitian operator. The variable K is the number of snapshots taken from the signal.

The conventional beamformer method estimates the spatial power spectrum for every possible AoA frequency as [7, eq. 3.43]

$$H_{ULA}(\psi, \theta) = \frac{\widetilde{\mathbf{a}}(\psi)\mathbf{R}\widetilde{\mathbf{a}}^H(\psi)}{\widetilde{\mathbf{a}}(\psi)\widetilde{\mathbf{a}}^H(\psi)}, \tag{5}$$

where $\widetilde{\mathbf{a}}(\psi)$ is the steering vector for all possible angles, as defined in (3). The angle ψ will be discretized into Q possible values, in other words there are Q steering frequencies. When the condition $\psi = \theta$ occurs, (5) reaches its maximum, which is the key assumption to estimate θ (the AoA of the direct line of sight component). It is important to note that the original AoA θ will be covered by the closest value of the Q possible steering angles. However as the number of Q increases (which is the case for Massive MIMO), the error associated with this discretization will be negligible.

For all the snapshots, the numerator of (4) can be written as

$$\widetilde{\mathbf{a}}(\theta)\mathbf{r}_k^H\mathbf{r}_k\widetilde{\mathbf{a}}^H(\theta) = \overline{\mathbf{q}_k}\mathbf{q}_k = |\mathbf{q}_k|^2. \tag{6}$$

where $\mathbf{q}_k = \mathbf{r}_k\widetilde{\mathbf{a}}^H(\theta)$.

Note that (6) presents the term $\mathbf{q}_k = \mathbf{r}_k\widetilde{\mathbf{a}}^H(\theta)$, that is exactly the spatial implementation of the Maximal Ratio Combining (MRC) principle [4], in which $\widetilde{\mathbf{a}}^H(\theta)$ is the spatial channel vector that optimizes the signal to noise ratio.

The MRC technique has been devised as the optimal combining technique since it maximizes the signal to noise ratio at the combiner output, however, in the Massive MIMO context, this technique has been used since the effect of the noise and fast fading vanish as the number of antennas is very large [1].

Other useful interpretation for (5) is the matched filter principle: a received signal is correlated with its template signal. The filter response is maximum when both signals are similar (i.e. correlated). In this particular case (5) could be seen as a spatial matching filter that gives a maximum response when the impinging signals (characterized on $\mathbf{R}$) match with the steering vector of the angle of origin $\widetilde{\mathbf{a}}(\theta)$.

A. URA CONFIGURATION MODEL

A similar model can be defined for the URA case. However, the URA array steering vector construction is different due to its two-dimensional characteristics as better explained in Appendix B. For this case, the spatial power spectrum is given as

$$H_{URA}(\psi,\xi)=\frac{\widetilde{\mathbf{a}}(\psi,\xi)\mathbf{R}\widetilde{\mathbf{a}}^{H}(\psi,\xi)}{\widetilde{\mathbf{a}}(\psi,\xi)\widetilde{\mathbf{a}}^{H}(\psi,\xi)}, \tag{7}$$

where $\widetilde{\mathbf{a}}(\psi,\xi)$ is given in (53) and (54). See Appendix B.

III. PROBLEM FORMULATION

The purpose of this work is to find the probability of detection for the conventional beamforming method for the ULA and URA geometries. Recalling equation (5), it is evident that the spatial spectrum depends on the steering angle and the real AoA, in other words, the original received signal $\mathbf{r}$ is transformed to the spatial frequency domain where the steering angles are the associated spatial frequencies. This fact is illustrated in Fig. 2.

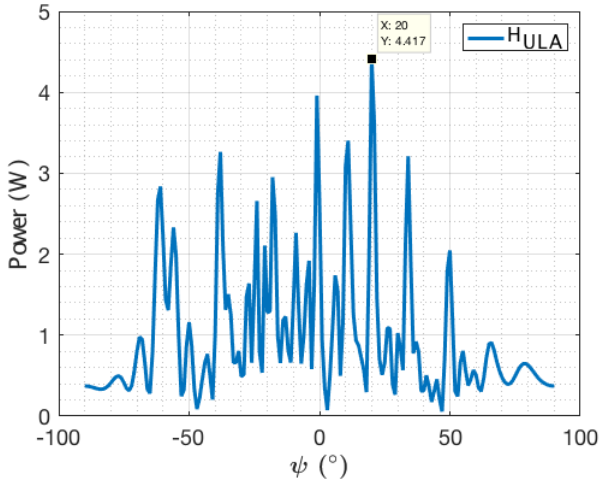

FIGURE 2. Spatial power spectrum of conventional beamforming with $\theta = 20°$, $Q = 181(\Delta_\psi = 1.0°)$, $K = 2$, $M = 50E$, $\sigma_n = 1$, $\sigma_f = 1$ for the ULA case.

Fig. 2 describes the relationship between power and angle, where the maximum occurs at $\psi = \theta = 20°$ which is the AoA of the direct line of sight component.

We define the probability of detection P_D as

$$P_D = \text{Prob}\left[\hat{\psi}=\theta\right]. \tag{8}$$

This circumstance occurs when the power of the associated frequency of $\psi = \theta$ is greater than the power of the rest of steering angles frequencies ψ. In other words

$$P_D = \text{Prob}\left[H_{ULA_{\theta,\theta}} > \{H_{ULA_{(\psi_1,\theta)}} \dots H_{ULA_{(\psi_{Q-1},\theta)}}\}\right], \tag{9}$$

where Q is the number of possible spatial steering frequencies.

It is important to emphasize, that in the strict sense, ψ will never be equal to θ since they are real variables. The probability of detection is a metric that is valid for a discrete problem and that is the reason for the discretization of ψ.

All further analysis will be performed using the random variable H_{ULA}. For the URA case, similar results are obtained since the geometry of URA does not affect the final behavior of our derivations. See Appendix B.

IV. PROBABILITY OF DETECTION

In order to get an expression for the Probability of Detection, we formulate two detection hypotheses

- H_0: $H_{ULA_{(\psi,\theta)}}$ has its maximum value at any angle frequency different from the real AoA, that is $\psi \neq \theta$.
- H_1: $H_{ULA_{(\psi,\theta)}}$ has its maximum value at the real AoA, that is $\psi = \theta$.

As it is shown in Appendix A, the random variable H_{ULA} defined in (5) turns out to be the sum of two squared Gaussian random variables. Each one of these variables corresponds to sum of M Gaussian random variables. For the hypothesis H_0, that is, for $\psi \neq \theta$ the mean of each Gaussian variate will be given by $\pi_1/\sqrt{M}$, and $\pi_2/\sqrt{M}$, where π_1 and π_2 are given in (39) and (40), respectively. As the number of antennas M goes to infinity, $\pi_1/\sqrt{M}$ and $\pi_2/\sqrt{M}$ tend to zero. Under this condition, H_{ULA} will be distributed according to a central *Chi*-squared distribution as

$$H_{ULA_{(\psi,\theta)}} = \frac{M\sigma_n^2+\sigma_f^2}{2KM}\Omega_{(\psi,\theta)}, \tag{10}$$

$$\Omega_{(\psi,\theta)} \sim \chi^2(2K). \tag{11}$$

where $\chi^2(\kappa)$ is the *Chi*-squared distribution [25] with parameter $\kappa > 0$. The PDF can be obtained and derived from (46) (Appendix A) as

$$f_{H_{ULA}}(x|H_0) = \left(\frac{KM}{M\sigma_n^2+\sigma_f^2}\right)^K \frac{x^{K-1}e^{-\frac{xKM}{M\sigma_n^2+\sigma_f^2}}}{\Gamma(K)}, \tag{12}$$

where $\Gamma(.)$ is the Gamma function [25], [26].

Under the hypothesis H_1, that is $\psi = \theta, \pi_1 = M$, and $\pi_2 = -M$, therefore $\pi_1/\sqrt{M}$ and $\pi_2/\sqrt{M}$ tend to $\sqrt{M}$ and $-\sqrt{M}$, respectively. Under this condition, the random variable H_{ULA} will be distributed according to a non-central *Chi*-squared as

$$H_{ULA}(\psi=\theta) = P_{ULA} = \frac{M\sigma_n^2+\sigma_f^2}{2KM}\Omega_{(\theta,\theta)}, \tag{13}$$

where

$$\Omega_{(\theta,\theta)} \sim \chi^2_{nc}\left(2K, \frac{4KM}{M\sigma_n^2+\sigma_f^2}\right). \quad (14)$$

The respective PDF is given in (47), as

$$f_{H_{ULA}}(x|H_1) = f_{P_{ULA}}(x) = \frac{KM}{M\sigma_n^2+\sigma_f^2} e^{-\frac{KM(x+2)}{M\sigma_n^2+\sigma_f^2}} \cdot \left(\frac{x}{2}\right)^{\frac{K-1}{2}} I_{K-1}\left(\frac{2KM}{M\sigma_n^2+\sigma_f^2}\sqrt{2x}\right), \quad (15)$$

where $I_c(d)$ is the modified Bessel function of the first kind with parameters $c \geq 0$ and $d \geq 0$ [25], [26].

The probability of a random variable X be less than other random variable Y, is defined as [25], [26]

$$\text{Prob}[X < Y] = \int_{-\infty}^{\infty}\left[\int_{-\infty}^{y} f_x(x)dx\right] f_y(y)dy \quad (16)$$

In our particular case, we want to know the probability of a set of $Q-1$ i.i.d. random variables X_i be less than a unique random variable Y, that is

$$\text{Prob}[\{X_1,\ldots,X_{Q-1}\} < Y] = \int_{-\infty}^{\infty}\left[\int_{-\infty}^{y} f_x(x)dx\right]^{Q-1} f_y(y)dy \quad (17)$$

The $Q-1$ probability density functions $f_x(x)$ are related to the hypothesis H_0 ($f_{H_{ULA}}(x|H_0)$) whereas the probability density function $f_y(y)$ is associated with the hypothesis H_1 ($f_{H_{ULA}}(x|H_1)$). Therefore, our probability of detection can be computed as

$$P_D = \text{Prob}[\{H_{ULA_{(\psi_1,\theta)}},\ldots,H_{ULA_{(\psi_{Q-1},\theta)}}\} < P_{ULA}], \quad (18)$$

or equivalently,

$$P_D = \int_0^{\infty}\left[\int_0^{y}\left(\frac{KM}{M\sigma_n^2+\sigma_f^2}\right)^K \frac{x^{K-1}e^{-\frac{xKM}{M\sigma_n^2+\sigma_f^2}}}{\Gamma(K)}dx\right]^{Q-1} \cdot \frac{KM}{M\sigma_n^2+\sigma_f^2} e^{-\frac{KM(y+2)}{M\sigma_n^2+\sigma_f^2}}\left(\frac{y}{2}\right)^{\frac{K-1}{2}} \cdot I_{K-1}\left(\frac{2KM}{M\sigma_n^2+\sigma_f^2}\sqrt{2y}\right)dy \quad (19)$$

The integral inside the brackets can be solved as

$$\int_0^{y}\left(\frac{KM}{M\sigma_n^2+\sigma_f^2}\right)^K \frac{x^{K-1}e^{-\frac{xKM}{M\sigma_n^2+\sigma_f^2}}}{\Gamma(K)}dx = 1 - \frac{\gamma\left(K, \frac{KMy}{M\sigma_n^2+\sigma_f^2}\right)}{\Gamma(K)}, \quad (20)$$

where $\gamma(\cdot,\cdot)$ is the incomplete Gamma function, and $\Gamma(\cdot)$ is the gamma function. Using (20) and the binomial identity $(x+a)^{Q-1} = \sum_{i=0}^{Q-1}\binom{Q-1}{i}x^i a^{Q-1-i}$, (19) can be written as

$$P_D = \int_0^{\infty}\sum_{i=0}^{Q-1}\binom{Q-1}{i}(-1)^{Q+i-1} \cdot \left(\frac{\gamma\left(K, \frac{KMy}{M\sigma_n^2+\sigma_f^2}\right)}{\Gamma(K)}\right)^{Q-1-i} \frac{KM}{M\sigma_n^2+\sigma_f^2} e^{-\frac{KM(y+2)}{M\sigma_n^2+\sigma_f^2}} \cdot \left(\frac{y}{2}\right)^{\frac{K-1}{2}} I_{K-1}\left(\frac{2KM}{M\sigma_n^2+\sigma_f^2}\sqrt{2y}\right)dy \quad (21)$$

Equation (21) has not a closed form expression, but it is numerically integrable. In the next section, this analytical expression will be compared to computer simulations.

V. NUMERICAL RESULTS

A. EQUIVALENT RANDOM VARIABLE

Fig. 3, and Fig. 4 show the analytical PDF and CDF, respectively, given in (46) and (47), and the equivalent simulated PDF and CDF for three different steering angles. As expected, both plots match perfectly, once that our analytical results are exact.

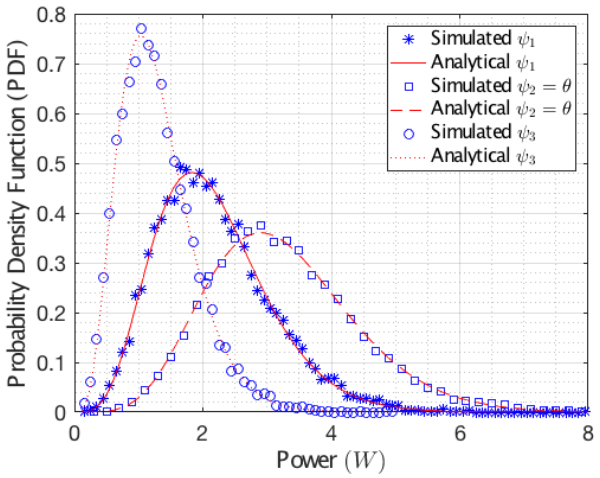

FIGURE 3. Normalized histogram for 10^4 realizations of (5) and analytical PDF given in (43), with $K = 5$, $M = 4$, $\sigma_f = 1$ and $\sigma_n = 1$ (SNR = 0 dB) for $\psi_1 = 15°$, $\psi_2 = \theta = 30°$ $\psi_3 = 70°$ in ULA case.

B. PROBABILITY OF DETECTION

We now focus on the probability of detection for Massive MIMO context, where a huge number of antennas are used for a particular application.

Fig. 5 shows that the probability of detection P_D is barely affected by the parameter M. Note the perfect agreement between simulation and the analytical result for values of M ($M \geq 50$), i.e., the Massive MIMO range.

Fig. 6 shows the probability of detection as a function of the number of snapshots. As it can be observed, the greater the number of snapshots K, the greater the probability of detection P_D. This behavior is expected since an increase in

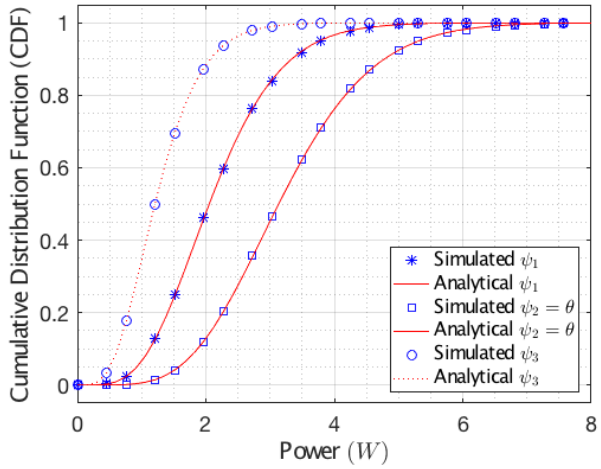

FIGURE 4. Associated CDF for 10^4 realizations of (5) and analytical CDF given in (44), with $K = 5$, $M = 4$, $\sigma_f = 1$ and $\sigma_n = 1$ (SNR = 0 dB) for $\psi_1 = 15°$, $\psi_2 = \theta = 30°$ $\psi_3 = 70°$ in ULA case.

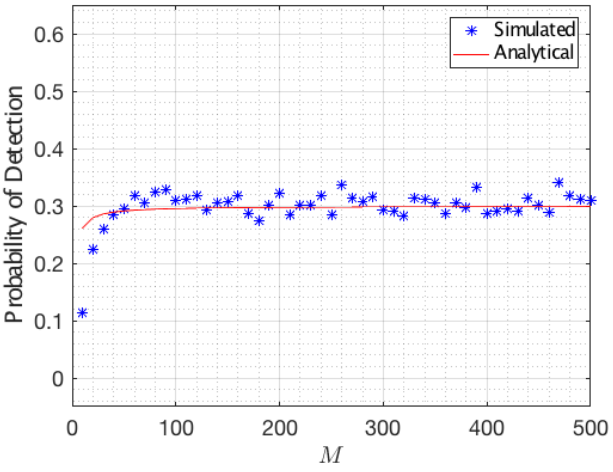

FIGURE 5. Probability of Detection with, $K = 2$, $Q = 121$ ($\Delta_\psi = 1.5°$), $\sigma_n = 1$, $\sigma_f = 1$ for ULA case.

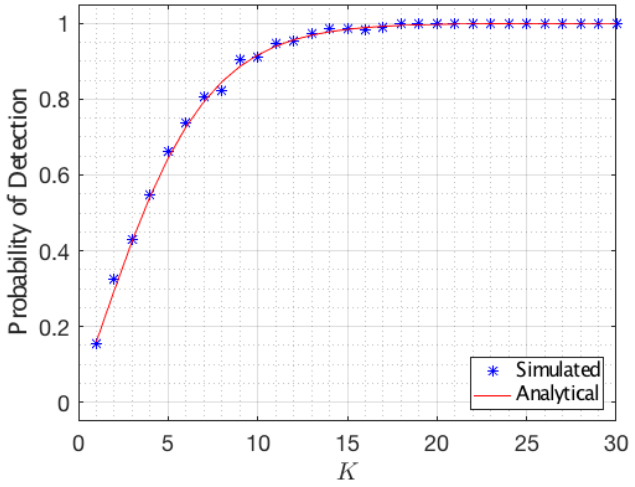

FIGURE 6. Probability of Detection with, $M = 100$, $Q = 121$ ($\Delta_\psi = 1.5°$), $\sigma_n = 1$, $\sigma_f = 1$ for ULA case.

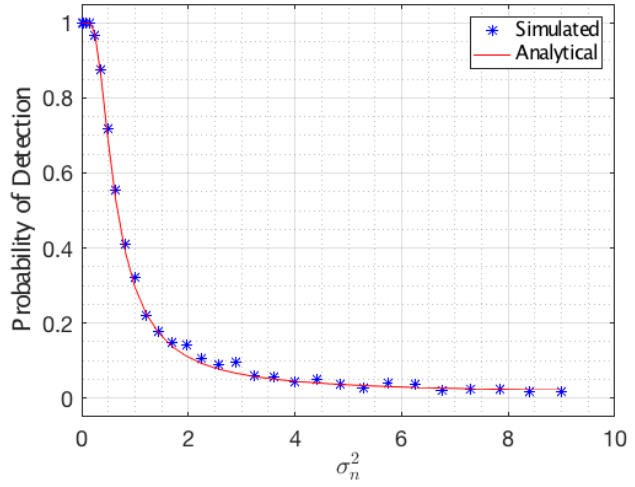

FIGURE 7. Probability of Detection with, $K = 2$, $M = 100$, $Q = 121$ ($\Delta_\psi = 1.5°$), $\sigma_f = 1$ for ULA case.

the number of snapshots can be considered equivalent to an increase in the signal to noise ratio. Note that the analytical and simulated curves are in close agreement.

Fig. 7 shows the probability of detection as a function of the power noise σ_n^2. Note that the absence of noise leads to a unitary probability of detection. Again, this figure validates our analytical results since there is no difference between the simulated and analytical curves.

C. RESOLUTION

The angle resolution is the angle step between the possible steering angles chosen to describe the AoA spatial spectrum. According to the beamforming principles, there is a maximum angular resolution that can be achieved for proper signal array processing [27]. This maximum is the denominated 3 dB beamwidth as

$$\Delta_{3dB} = \Delta_\psi = \frac{2}{M}, \tag{22}$$

This approximation is set for isotropic antennas, large number of antennas, and antenna spacing equals to $d = \frac{\lambda}{2}$, as stated in section II. The maximum number, Q, of possible angles should obey the following inequality

$$Q = \frac{S}{\Delta_\psi}, \tag{23}$$

where S is the span of the steering angles. In our case the range is set as $\{-\frac{\pi}{2}$ to $\frac{\pi}{2}\}$ in order to avoid angle ambiguity. Therefore

$$Q = \frac{\frac{\pi}{2} - \left(-\frac{\pi}{2}\right)}{\Delta_\psi} = \frac{\pi}{\Delta_\psi}, \tag{24}$$

so finally, replacing (22) into (24), we get the condition

$$Q < \frac{\pi}{2} M. \tag{25}$$

In the simulation scenario, we have established $M = 100$, therefore $Q < 157.07$. The results shown in subsection V-B have considered this restriction.

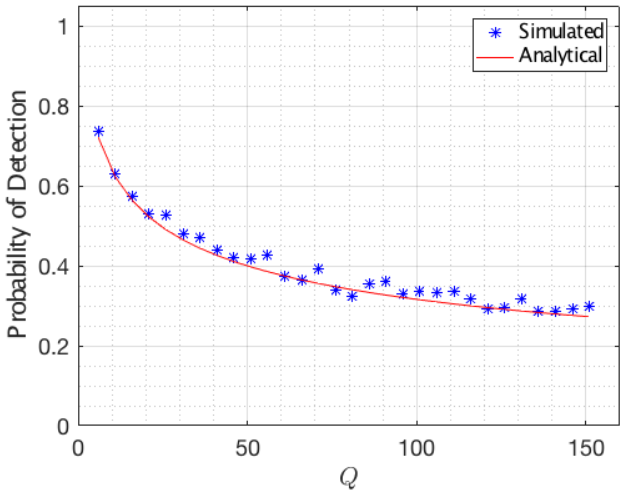

FIGURE 8. Probability of Detection with, $K = 2$, $M = 100$, $\sigma_n = 1$, $\sigma_f = 1$ for ULA case.

Fig. 8 shows the probability of detection versus the number of possible angles Q. Note that the probability of detection decreases as the number of possible angles Q increases. But it is also interesting to observe that there is a floor in the probability of detection suggesting the existence of a lower limit.

VI. CONCLUSIONS

We derived the exact analytical probability of detection for conventional beamforming on ULA and URA geometries considering fading and noise scenarios in a massive MIMO context. The resulting equation is related to a scaled non-central *Chi-squared* random variable and its associated PDF and CDF. Our simulated and analytical curves matched perfectly, corroborating the analytical derivations. The number of snapshots, K, and the number of antennas, M, have a great impact on the probability of detection and therefore in the estimation angle. It has been observed that these parameters can mitigate the effects of fading and noise. Particularly, in conventional beamforming, a large number of antennas improved the probability of detection which is the case for the Massive MIMO technique. The parameter K has an influence on the variance of the associated random variable H_{ULA}, but it does not affect its mean. The probability of Detection for URA geometry presented similar behavior as the ULA geometry, except that the parameter M must be substituted by the parameter $M_x M_y$ in all equations. The advantage of the URA geometry over the ULA geometry is the possibility of 3D AoA estimation (elevation and azimuth angles).

APPENDIX A//EQUIVALENT RANDOM VARIABLE FOR ULA

Note that (5), evaluated for a fixed angle, is a random variable (here simplified as $H_{ULA}(\psi,\theta) = H_{ULA}$ and $\widetilde{\mathbf{a}}(\psi) = \widetilde{\mathbf{a}}_\psi = \frac{\mathbf{a}_\psi}{\sqrt{M}}$, defined as

$$H_{ULA} = \frac{\widetilde{\mathbf{a}}_\psi \mathbf{R}\widetilde{\mathbf{a}}_\psi^H}{\widetilde{\mathbf{a}}_\psi \widetilde{\mathbf{a}}_\psi^H} = \frac{\mathbf{a}_\psi \mathbf{R}\mathbf{a}_\psi^H}{\mathbf{a}_\psi \mathbf{a}_\psi^H} = \frac{\mathbf{a}_\psi \mathbf{R}\mathbf{a}_\psi^H}{M}, \tag{26}$$

We start from $\mathbf{r}_k$ (2)

$$\mathbf{r}_k = \widetilde{\mathbf{a}}_\theta \circ \mathbf{h}_k s(t) + \mathbf{n}_k, \tag{27}$$

where r_{ki} is the i-th element of $\mathbf{r}_k$, and a_{θ_i} is the i-th element of $\widetilde{\mathbf{a}}_\theta$. Since the sum of complex Gaussian random variables is also Gaussian distributed, the real and imaginary part of r_{ki} are distributed as

$$\Re(r_{ki}) \sim N\left(\frac{\cos\left(i\frac{2\pi\Delta}{\lambda}\sin(\theta)\right) - \sin\left(i\frac{2\pi\Delta}{\lambda}\sin(\theta)\right)}{\sqrt{M}}, \frac{M\sigma_n^2+\sigma_f^2}{2M}\right), \tag{28}$$

$$\Im(r_{ki}) \sim N\left(\frac{\cos\left(i\frac{2\pi\Delta}{\lambda}\sin(\theta)\right) + \sin\left(i\frac{2\pi\Delta}{\lambda}\sin(\theta)\right)}{\sqrt{M}}, \frac{M\sigma_n^2+\sigma_f^2}{2M}\right), \tag{29}$$

where the notation $N\left(\mu,\sigma^2\right)$ stands for a normal distribution with mean μ and variance σ^2.

Inserting (4) into (26), we get

$$H_{ULA} = \frac{1}{KM}\sum_{k=0}^{K-1} \mathbf{a}_\psi \mathbf{r}_k^H \mathbf{r}_k \mathbf{a}_\psi^H. \tag{30}$$

Now, we can define the variable $\mathbf{q}_k$ as

$$\mathbf{q}_k = \mathbf{a}_\psi \mathbf{r}_k^H = \Re(\mathbf{q}_k) + j\Im(\mathbf{q}_k). \tag{31}$$

Therefore

$$\mathbf{a}_\psi \mathbf{r}_k^H \mathbf{r}_k \mathbf{a}_\psi^H = \Re(\mathbf{q}_k)^2 + \Im(\mathbf{q}_k)^2, \tag{32}$$

which can be expanded as

$$\begin{aligned}\mathbf{a}_\psi \mathbf{r}_k^H \mathbf{r}_k \mathbf{a}_\psi^H = &\left(\sum_{i=0}^{M-1} \cos\left(i\frac{2\pi\Delta}{\lambda}\sin(\psi)\right)\Re(r_{ki})\right.\\ &\left. + \sin\left(i\frac{2\pi\Delta}{\lambda}\sin(\psi)\right)\Im(r_{ki})\right)^2\\ &+ \left(\sum_{i=0}^{M-1} -\cos\left(i\frac{2\pi\Delta}{\lambda}\sin(\psi)\right)\Im(r_{ki})\right.\\ &\left. + \sin\left(i\frac{2\pi\Delta}{\lambda}\sin(\psi)\right)\Re(r_{ki})\right)^2.\end{aligned} \tag{33}$$

Note that all the terms inside the summation are Gaussian distributed since r_{ki} is Gaussian and a_{ψ_i} is a constant. Also, the real and imaginary part of r_{ki} are independent. Now defining the new Gaussian variables as

$$u_{ki} = \cos\left(i(2\pi\Delta/\lambda)\sin(\psi)\right)\Re(r_{ki}) \tag{34}$$

$$\delta_{ki} = \sin\left(i(2\pi\,\Delta/\lambda)\sin(\psi)\right)\Im(r_{ki}), \tag{35}$$

$$\eta_{ki} = \sin\left(i(2\pi\,\Delta/\lambda)\sin(\psi)\right)\Re(r_{ki}) \tag{36}$$

$$\zeta_{ki} = \cos\left(i(2\pi\,\Delta/\lambda)\sin(\psi)\right)\Im(r_{ki}) \tag{37}$$

then we can write (33) as

$$\mathbf{a}_\psi \mathbf{r}_k^H \mathbf{r}_k \mathbf{a}_\psi^H = \left(\sum_{i=0}^{M-1} u_{ki} + \delta_{ki}\right)^2 + \left(\sum_{i=0}^{M-1} \eta_{ki} - \zeta_{ki}\right)^2. \tag{38}$$

The terms inside the sum are also Gaussian distributed, thus

$$\sum_{i=0}^{M-1} u_{ki} + \delta_{ki} \sim N\left(\frac{1}{\sqrt{M}}\cdot\pi_1, \frac{M\sigma_n^2+\sigma_f^2}{2}\right), \tag{39}$$

$$\sum_{i=0}^{M-1} \eta_{ki} - \zeta_{ki} \sim N\left(\frac{1}{\sqrt{M}}\cdot\pi_2, \frac{M\sigma_n^2+\sigma_f^2}{2}\right), \tag{40}$$

where (after trigonometrical reduction)

$$\pi_1 = \sum_{i=0}^{M-1} \cos\left(i\frac{2\pi\,\Delta}{\lambda}\Xi\right) + \sin\left(i\frac{2\pi\,\Delta}{\lambda}\Xi\right) \tag{41}$$

$$\pi_2 = \sum_{i=0}^{M-1} \sin\left(i\frac{2\pi\,\Delta}{\lambda}\Xi\right) - \cos\left(i\frac{2\pi\,\Delta}{\lambda}\Xi\right) \tag{42}$$

$$\Xi = \sin(\psi) - \sin(\theta) \tag{43}$$

Since the sum of independent non-central square Gaussians with $\sigma^2 = 1$ is a non-central *Chi*-squared distributed random variable, we finally get that (30) (after unitary variance normalization) can be written as

$$H_{ULA} = \frac{M\sigma_n^2+\sigma_f^2}{2KM}\Omega_{(\psi,\theta)}, \tag{44}$$

where

$$\Omega_{(\psi,\theta)} \sim \chi_{nc}^2\left(2K, \frac{2K\left(\pi_1^2+\pi_2^2\right)}{M\left(M\sigma_n^2+\sigma_f^2\right)}\right), \tag{45}$$

and $\chi_{nc}^2(\kappa,\lambda)$ is the non-central *Chi*-squared distribution [25] with parameters $\kappa > 0$ and $\lambda > 0$. This result shows that the spatial power spectrum given in (5) has an equivalent random variable, which depends on the spatial frequency related to the angles ψ and θ.

The derived PDF for H_{ULA} is given as

$$f_{H_{ULA}}(x) = \frac{KM}{M\sigma_n^2+\sigma_f^2} e^{-\frac{K\left(M^2x+\pi_1^2+\pi_2^2\right)}{M\left(M\sigma_n^2+\sigma_f^2\right)}} \cdot \left(\frac{M^2x}{\left(\pi_1^2+\pi_2^2\right)}\right)^{\frac{K-1}{2}} I_{K-1}\left(\frac{2K}{M\sigma_n^2+\sigma_f^2}\sqrt{\left(\pi_1^2+\pi_2^2\right)x}\right), \tag{46}$$

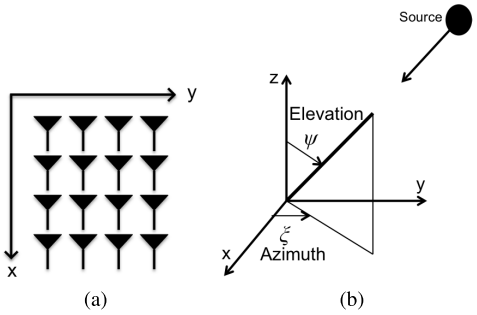

FIGURE 9. URA characteristics. (a) Layout deployment. (b) Angle incidence.

where $I_c(d)$ is the modified Bessel function of the first kind with parameters $c \geq 0$ and $d \geq 0$. The corresponding CDF can be found as

$$F_{H_{ULA}}(x) = 1 - Q_K\left(\sqrt{\frac{2K\left(\pi_1^2+\pi_2^2\right)}{M\left(M\sigma_n^2+\sigma_f^2\right)}}, \sqrt{\frac{2KM}{M\sigma_n^2+\sigma_f^2}x}\right), \tag{47}$$

where $Q_e(a,b)$ is the Marcum-Q function with parameters $a \geq 0$, $b \geq 0$ and $e \geq 0$.

The mean and the variance of the random variable H_{ULA} can be computed respectively as (by the non-central *Chi*-squared distribution properties [25], [26])

$$\mathbf{E}[H_{ULA}] = \frac{M\left(M\sigma_n^2+\sigma_f^2\right)+\pi_1^2+\pi_2^2}{M^2}, \tag{48}$$

$$\mathbf{var}[H_{ULA}] = \frac{(M\sigma_n^2+\sigma_f^2)\left[M\left(M\sigma_n^2+\sigma_f^2\right)+2\left(\pi_1^2+\pi_2^2\right)\right]}{KM^3}. \tag{49}$$

APPENDIX B//EQUIVALENT RANDOM VARIABLE FOR URA

URA configuration uses an extra angle dimension where the array is located at the *xy* plane, with the first element placed at the origin (see Fig. 9). In this way, the elevation and azimuth steering vectors of the impinging signal in the array are given as

$$\mathbf{a}_u(\psi,\xi) = \left[1\; e^{ju} \ldots e^{j(M_x-1)u}\right], \tag{50}$$

$$\mathbf{a}_v(\psi,\xi) = \left[1 e^{jv} \ldots e^{j(M_y-1)v}\right], \tag{51}$$

where $u = -(2\pi/\lambda)\Delta\sin(\psi)\sin(\xi)$, and $v = -(2\pi/\lambda)\Delta\sin(\psi)\cos(\xi)$. These vectors are multiplied to get a matrix $\mathbf{A}(\psi,\xi)$ as

$$\mathbf{A}(\psi,\xi) = \mathbf{a}_v^H(\psi,\xi)\mathbf{a}_u(\psi,\xi). \tag{52}$$

Then matrix $\mathbf{A}(\psi,\xi)$ is transformed into a $1 \times M_xM_y$ vector using the vec $(\cdot)$ operation

$$\mathbf{a}(\psi,\xi) = \mathrm{vec}\left[\mathbf{A}(\psi,\xi)\right]. \tag{53}$$

$$\widetilde{\mathbf{a}}(\psi,\xi)=\frac{\mathbf{a}(\psi,\xi)}{\sqrt{M_xM_y}}. \tag{54}$$

Note that, from (27), $\mathbf{r}_k$ has the same dimension as $\widetilde{\mathbf{a}}(\psi,\xi)$, therefore the new dimension of $\mathbf{r}_k$ will be $1\times M_xM_y$. Consequently, (7) becomes

$$H_{URA}(\psi,\xi)=\frac{\widetilde{\mathbf{a}}_{\psi,\xi}\mathbf{R}\widetilde{\mathbf{a}}^H_{\psi,\xi}}{\widetilde{\mathbf{a}}_{\psi,\xi}\widetilde{\mathbf{a}}^H_{\psi,\xi}}=\frac{\mathbf{a}_{\psi,\xi}\mathbf{R}\mathbf{a}^H_{\psi,\xi}}{\mathbf{a}_{\psi,\xi}\mathbf{a}^H_{\psi,\xi}}=\frac{\mathbf{a}_{\psi,\xi}\mathbf{R}\mathbf{a}^H_{\psi,\xi}}{M_xM_y} \tag{55}$$

Where the dimension of matrix $\mathbf{R}$ will be given as $M_xM_y\times M_xM_y$. Furthermore, $\widetilde{\mathbf{a}}_{\theta,\phi}=\widetilde{\mathbf{a}}(\psi=\theta,\xi=\phi)$ is used in (26) and (27). The following steps will henceforth the same as in the ULA case, just replacing the parameter M by M_xM_y and $a_{(\theta_i)}$ by $a_{(\psi,\xi_i)}$. Finally, equations (41) and (42) can be written as

$$\begin{aligned}\pi_1=&\sum_{i=0}^{M_xM_y-1}\Re(a_{(\psi,\xi)_i})\left(\Re(a_{(\theta,\phi)_i})-\Im(a_{(\theta,\phi)_i})\right)\\&+\Im(a_{(\psi,\xi)_i})\left(\Re(a_{(\theta,\phi)_i})+\Im(a_{(\theta,\phi)_i})\right),\end{aligned} \tag{56}$$

$$\begin{aligned}\pi_2=&\sum_{i=0}^{M_xM_y-1}\Im(a_{(\psi,\xi)_i})\left(\Re(a_{(\theta,\phi)_i})-\Im(a_{(\theta,\phi)_i})\right)\\&-\Re(a_{(\psi,\xi)_i})\left(\Re(a_{(\theta,\phi)_i})+\Im(a_{(\theta,\phi)_i})\right).\end{aligned} \tag{57}$$

ACKNOWLEDGMENT

The authors thank all the people that helped in the development of this work: Michel Yacoub, Paulo Cardieri, Richard Demo, Santosh Kumar, Natalia Bernardes, Camilo Osorio, Loren Forero, Alessandro de Oliveira, Melissa Munoz, Yalena Narvaez, and Ruby Bravo.

REFERENCES

[1] E. G. Larsson, O. Edfors, F. Tufvesson, and T. L. Marzetta, "Massive MIMO for next generation wireless systems," *IEEE Commun. Mag.*, vol. 52, no. 2, pp. 186–195, Feb. 2014.
[2] L. Xu, J. Wang, H. Zhang, and T. A. Gulliver, "Performance analysis of IAF relaying mobile D2D cooperative networks," *J. Franklin Inst.*, vol. 354, no. 2, pp. 902–916, Jan. 2017. [Online]. Available: http://www.sciencedirect.com/science/article/pii/S0016003216303908
[3] L. Xu, H. Zhang, J. Wang, and T. A. Gulliver, "Joint TAS/SC and power allocation for IAF relaying D2D cooperative networks," *Wireless Netw.*, vol. 23, no. 7, pp. 2135–2143, 2017.
[4] T. L. Marzetta, "Noncooperative cellular wireless with unlimited numbers of base station antennas," *IEEE Trans. Wireless Commun.*, vol. 9, no. 11, pp. 3590–3600, Nov. 2010.
[5] N. Garcia, H. Wymeersch, E. G. Larsson, A. M. Haimovich, and M. Coulon, "Direct localization for massive MIMO," *IEEE Trans. Signal Process.*, vol. 65, no. 10, pp. 2475–2487, May 2017.
[6] D. Dardari, C.-C. Chong, and M. Z. Win, "Threshold-based time-of-arrival estimators in UWB dense multipath channels," *IEEE Trans. Commun.*, vol. 56, no. 8, pp. 1366–1378, Aug. 2008.
[7] Z. Chen, G. Gokeda, and Y. Yu, *Introduction to Direction-Of-Arrival Estimation* (Artech House Remote Sensing Library), 1st ed. Norwood, MA, USA: Artech House, 2010.
[8] M.-J. Wang, J.-L. Cai, F.-S. Tseng, and C.-Y. Hsu, "A low-complexity 2-D angle of arrival estimation in massive MIMO systems," in *Proc. Int. Comput. Symp. (ICS)*, Dec. 2016, pp. 710–713.
[9] M. Li, Y. Lu, and B. He, "Array signal processing for maximum likelihood direction-of-arrival estimation," *J. Elect. Electron. Syst.*, vol. 3, no. 1, p. 117, 2014.
[10] Y. Fan, J. B. Li, H. Li, and C. Tian, "A stochastic framework of millimeter wave signal for mobile users: Experiment, modeling and application in beam tracking," in *Proc. 11th Global Symp. Millim. Waves (GSMM)*, May 2018, pp. 1–6.
[11] M. B. Zeytinci, V. Sari, F. K. Harmanci, E. Anarim, and M. Akar, "Location estimation using RSS measurements with unknown path loss exponents," *EURASIP J. Wireless Commun. Netw.*, vol. 2013, no. 1, p. 178, Jun. 2013, doi: 10.1186/1687-1499-2013-178.
[12] V. Savic and E. Larsson, "Fingerprinting-based positioning in distributed massive MIMO systems," in *Proc. IEEE 82nd Veh. Tech. Conf. (VTC Fall)*, Sep. 2015, pp. 1–5.
[13] M. W. Khan, N. Salman, and A. H. Kemp, "Cooperative positioning using angle of arrival and time of arrival," in *Proc. Sensor Signal Process. Defence (SSPD)*, Sep. 2014, pp. 1–5.
[14] A. Beck, P. Stoica, and J. Li, "Exact and approximate solutions of source localization problems," *IEEE Trans. Signal Process.*, vol. 56, no. 5, pp. 1770–1778, May 2008.
[15] L. Zhang, Y. H. Chew, and W.-C. Wong, "A novel angle-of-arrival assisted extended Kalman filter tracking algorithm with space-time correlation based motion parameters estimation," in *Proc. 9th Int. Wireless Commun. Mobile Comput. Conf. (IWCMC)*, Jul. 2013, pp. 1283–1289.
[16] S.-H. Fang and C.-H. Wang, "A dynamic hybrid projection approach for improved Wi-Fi location fingerprinting," *IEEE Trans. Veh. Technol.*, vol. 60, no. 3, pp. 1037–1044, Mar. 2011.
[17] J. Capon, "High-resolution frequency-wavenumber spectrum analysis," *Proc. IEEE*, vol. 57, no. 8, pp. 1408–1418, Aug. 1969.
[18] R. O. Schmidt, "Multiple emitter location and signal parameter estimation," *IEEE Trans. Antennas Propag.*, vol. AP-34, no. 3, pp. 276–280, Mar. 1986.
[19] R. Roy and T. Kailath, "Esprit-estimation of signal parameters via rotational invariance techniques," *IEEE Trans. Acoust., Speech, Signal Process.*, vol. 37, no. 7, pp. 984–995, Jul. 1989.
[20] J. Salmi and A. F. Molisch, "Propagation parameter estimation, modeling and measurements for ultrawideband MIMO radar," *IEEE Trans. Antennas Propag.*, vol. 59, no. 11, pp. 4257–4267, Nov. 2011.
[21] R. J. Muirhead, *Aspects of Multivariate Statistical Theory*, 2nd ed. Hoboken, NJ, USA: Wiley, 2005.
[22] G. Xu, R. H. Roy, III, and T. Kailath, "Detection of number of sources via exploitation of centro-symmetry property," *IEEE Trans. Signal Process.*, vol. 42, no. 1, pp. 102–112, Jan. 1994.
[23] Y. L. C. D. Jong and M. H. A. J. Herben, "High-resolution angle-of-arrival measurement of the mobile radio channel," *IEEE Trans. Antennas Propag.*, vol. 47, no. 11, pp. 1677–1687, Nov. 1999.
[24] M. R. J. A. E. Kwakkernaat, Y. L. C. D. Jong, R. J. C. Bultitude, and M. H. A. J. Herben, "High-resolution angle-of-arrival measurements on physically-nonstationary mobile radio channels," *IEEE Trans. Antennas Propag.*, vol. 56, no. 8, pp. 2720–2729, Aug. 2008.
[25] A. Papoulis and S. Pillai, *Probability, Random Variables and Stochastic Processes* (McGraw-Hill Electrical and Electronic Engineering Series). 4th ed. New York, NY, USA: McGraw-Hill, 2002.
[26] S. Kay, *Intuitive Probability and Random Processes using MATLAB*, 1st ed. New York, NY, USA: Springer, 2006.
[27] M. Richards, *Fundamentals of Radar Signal Processing* (Professional Engineering). New York, NY, USA: McGraw-Hill, 2005.

CLAUDIO ALFONSO BOHÓRQUEZ CAMARGO was born in Chiquinquirá, Boyacá, Colombia. He graduated in electronics engineering and in electrical engineering from the National University of Colombia, Bogotá, Colombia, in 2011 and 2012, respectively. He received the M.Sc. degree from the State University of Campinas, UNICAMP, Brazil, in 2018. He worked for four years in the petrochemical industry as an instrumentation and automation specialist. His research interests are wireless communications, radar and industrial instrumentation, and automation.

GUSTAVO FRAIDENRAICH graduated in electrical engineering from the Federal University of Pernambuco, UFPE, Brazil, in 1997. He received the M.Sc. and Ph.D. degrees from the State University of Campinas, UNICAMP, Brazil, in 2002 and 2006, respectively. From 2006 to 2008, he was a Post-Doctoral Fellow at Stanford University (Star Lab Group), USA. He is currently an Assistant Professor at UNICAMP. His research interests include multiple antenna systems, cooperative systems, radar systems, and wireless communications in general. He was a recipient of the Fundação de Amparo à Pesquisa do Estado de São Paulo Young Researcher Scholarship in 2009. He has been associated editor of the ETT journal for many years.

LUCIANO LEONEL MENDES received the B.Sc. and M.Sc. degrees in electrical engineering from Inatel, Brazil, in 2001 and 2003, respectively, and the Ph.D. degree in electrical engineering from UNICAMP, Brazil, in 2007. Since 2001, he has been a Professor at Inatel, where he has acted as a Technical Manager of the Hard-Ware Development Laboratory from 2006 to 2012. He has coordinated the Master Program at Inatel and several research projects funded by FAPEMIG, FINEP, and BNDES. He has been a Post-Doctoral Visiting Researcher, sponsored by CNPq-Brazil, at Vodafone Chair Mobile Communications Systems, TU Dresden, since 2013. His main area of research is wireless communication, and currently, he is involved in multicarrier modulations for 5G networks and future mobile communication systems.